

Induced superfluidity of imbalanced Fermi gases near unitarity

Kelly R. Patton^{1,*} and Daniel E. Sheehy^{2,†}

¹*Seoul National University, Department of Physics and Astronomy
Center of Theoretical Physics, 151-747 Seoul, Korea*

²*Department of Physics and Astronomy, Louisiana State University, Baton Rouge, Louisiana 70803
(Dated: March 28, 2012)*

The induced intraspecies interactions among the majority species, mediated by the minority species, is computed for a population-imbalanced two-component Fermi gas. Although the Feshbach-resonance mediated interspecies interaction is dominant for equal populations, leading to singlet s -wave pairing, we find that in the strongly imbalanced regime the induced intraspecies interaction leads to p -wave pairing and superfluidity of the majority species. Thus, we predict that the observed spin-polaron Fermi liquid state in this regime is unstable to p -wave superfluidity, in accordance with the results of Kohn and Luttinger, below a temperature that, near unitarity, we find to be within current experimental capabilities. Possible experimental signatures of the p -wave state using radio-frequency spectroscopy as well as density-density correlations after free expansion are presented.

PACS numbers: 05.30.Fk, 03.75.Ss, 67.85.-d, 32.30.Bv

I. INTRODUCTION

The extraordinary variety of tunable “knobs” in cold atomic gas experiments has yielded a wide assortment of correlated phases of matter ranging from superfluid and Mott insulating phases of bosonic atoms, to superfluid and nonsuperfluid phases of fermionic atoms [1–4]. In the fermionic case the experimentally available knobs include the interactions among two species of fermion, their relative densities [5–8], and also the effective spatial dimension, which can be controlled via an appropriate confining trapping potential.

Our present focus is on the case of a three-dimensional two-species Fermi gas (labeled by the spin index $\sigma = \uparrow, \downarrow$) interacting via a magnetic field-tuned Feshbach resonance. In the balanced case of equal densities of the two species, and as a function of the Feshbach resonance detuning that essentially controls $\frac{1}{a_s}$ with a_s the s -wave scattering length, the atomic gas undergoes the well-known crossover from a Bose-Einstein condensate (BEC) of tightly bound molecular pairs at $\frac{1}{k_F a_s} \gtrsim 1$, through the strongly correlated unitary regime at $\frac{1}{k_F a_s} \simeq 0$, to a weakly coupled Bardeen-Cooper-Schrieffer (BCS) superconductor of Cooper pairs at $\frac{1}{k_F a_s} \lesssim -1$. Here, $k_F \propto n^{1/3}$ is the Fermi wavevector (with n the total density), the inverse of which characterizes the typical interparticle spacing. Importantly, the low-temperature state of this balanced Fermi gas is believed to undergo no symmetry-changing phase transitions as the BEC-BCS crossover is traversed.

The behavior of strongly interacting 3D Fermi gases in the *imbalanced* case is considerably richer, with numerous phases having been predicted [9–16] to occur (as recently

reviewed in Refs. 17, 18), including the long sought-after Fulde-Ferrell-Larkin-Ovchinnikov (FFLO) state [19, 20], in which the superfluid spontaneously develops a spatial modulation in the local pairing amplitude to accommodate the excess fermions of the majority species [21–23]. Unfortunately, the FFLO phase has not yet been observed in 3D imbalanced Fermi gases (although evidence for a 1D analogue of this state has been found [24]). Instead, under an imposed density imbalance, characterized by the population imbalance $P = \frac{n_\uparrow - n_\downarrow}{n_\uparrow + n_\downarrow}$ (note we always assume the densities n_σ of species σ satisfy $n_\uparrow \geq n_\downarrow$), interacting Fermi gases enter a regime of phase separation at moderate P followed by an imbalanced nonsuperfluid phase at large P , as seen in the phase diagram Fig. 1.

In the strongly imbalanced limit ($P \rightarrow 1^-$) our system amounts to considering the phase resulting from adding a few spins- \downarrow to a Fermi sea of the spins- \uparrow . In this strongly imbalanced regime, within the simplest picture there are two possible fates of such an added spin down: It can either form a molecular bound state with one spin- \uparrow , or it can remain unpaired. In the former case, occurring at $a_s > 0$ but $k_F a_s \lesssim 1$ (i.e. the BEC limit), as more spins- \downarrow are added more molecules will develop and, presumably, condense. Our interest is in the latter regime, in which (within this simple picture) no interspecies pairing occurs and condensation is suppressed.

From one point of view, the inability to establish pairing in this regime is simply traced to the fact that, with an imposed density imbalance, not all the majority spins- \uparrow have a minority spin- \downarrow fermion to pair with. More precisely, the presence of a density imbalance implies a concomitant Fermi surface (and Fermi energy) mismatch, so that the formation of low-energy Fermi surface pairing correlations is interrupted, leaving an imbalanced interacting Fermi liquid state [25–27] that, apparently, lacks any superfluid order even at low temperatures.

How do the strong attractive interspecies interactions manifest themselves, given the inability of this system to form s -wave Cooper pairs and condense? Recent experi-

*kpatton@physast.uga.edu

†sheehy@phys.lsu.edu

ments show evidence of the formation of Fermi polarons, in which a cloud of the spins- \uparrow form around each spin- \downarrow , leading to an observable shift in the spin- \downarrow chemical potential [28, 29] in agreement with theoretical predictions [30–32]. The central question studied here concerns whether, at $T \rightarrow 0$, this polaron phase of matter persists or whether another broken-symmetry phase emerges.

One motivation for this possibility is the well-known results of Kohn and Luttinger [33, 34], who showed that interacting Fermi liquid phases are generally unstable to pairing in some angular momentum channel at low T . Given that the polaron state of imbalanced Fermi gases is, at its heart, essentially a Fermi liquid for both species (exhibiting, for example, a sharp Migdal discontinuity in the momentum occupation at the Fermi surface), we generally expect the Kohn-Luttinger mechanism to hold, yielding odd angular momentum *intraspecies* Cooper pairing at both the spin- \uparrow and spin- \downarrow Fermi surfaces for $T \rightarrow 0$ [35, 36]. The odd-angular momentum pairing requirement follows from the Pauli exclusion principle; while the simplest such state has p -wave symmetry (assumed here), more generally any odd ℓ is possible.

In fact, p -wave pairing is also possible in the deep BEC limit of imbalanced gases via a somewhat different mechanism [35, 37]. As noted above, in the deep BEC limit tightly bound molecular pairs form even at very large imbalance (only vanishing when $n_{\downarrow} \rightarrow 0$). If we imagine decreasing P from unity in this limit, within a mean-field picture two possibilities emerge [12, 14, 15]: Firstly, the system can form a homogeneous polarized magnetic superfluid phase (SF_M in Fig. 1), in which such molecular pairs coexist with a Fermi sea of the excess spins- \uparrow . This possibility is found in the very deep BEC limit (i.e., $\frac{1}{k_F a_s} > 2.37$ within mean-field theory, with the tricritical point of Fig. 1 becoming a quantum tricritical point [14] at $\frac{1}{k_F a_s} = 2.37$). Secondly, closer to unitarity, the system can form a phase separated mixture of SF_M and imbalanced normal phase. Our point here is that, in the SF_M phase, p -wave pairing can be induced among the excess spins- \uparrow by the molecular bosons, a mechanism studied in Refs. [35, 37]. Here, we work away from the regimes of phase separation and SF_M, focusing on induced pairing of the spins- \uparrow mediated purely by the presence of the spins- \downarrow (i.e., without any molecular pairing); however, the relationship between these two regimes is an interesting problem for future research.

In this paper we present the details of our calculation of the transition temperature below which p -wave pairing is expected to occur within this mechanism, expanding upon our recent Rapid Communication [36]. This calculation can be summarized by the phase diagram Fig. 1 for imbalanced Fermi gases at unitarity, showing regions of polaron Fermi liquid, imbalanced or “magnetic” superfluid SF_M, and phase separation. Here, the first-order phase boundary enclosing the regime of phase separation and the second-order phase boundary separating the SF_M and polaron Fermi liquid phases are only sketched (i.e. are not the result of a calculation). However, we drew

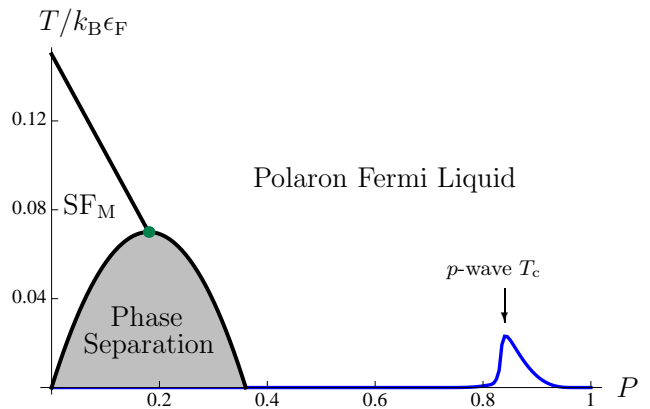


FIG. 1: (Color online) Proposed phase diagram of population imbalanced Fermi gases, at unitarity $\frac{1}{k_F a_s} = 0$, as a function of temperature T (normalized to the Fermi energy ϵ_F multiplied by the Boltzmann constant k_B) and population imbalance P , showing regions of imbalanced superfluid SF_M, phase separation (at temperatures below the tricritical point, a solid dot (green online) [14, 42, 43]) polaron Fermi liquid, and a p -wave paired state. The principal question is whether the polaron Fermi liquid phase, in which both spins- \uparrow and spins- \downarrow possess Fermi surfaces (despite the strong interactions), persist to $T \rightarrow 0$. The black phase boundaries are only sketched but consistent with the experimentally determined phase diagram of Ref. 38. Below the blue curve, derived here, we find an instability towards p -wave pairing of the spin- \uparrow Fermi surface.

these phase boundaries to be consistent with the experimental results of Ref. 38 to illustrate the fact that our maximum predicted transition temperature for p -wave pairing (solid curve, blue online) is not much smaller than the temperature scales characterizing these phase boundaries, suggesting that it may be possible to observe p -wave pairing of strongly imbalanced Feshbach-resonant Fermi gases.

We remark that other recent work has considered the effect of intraspecies interactions in imbalanced Fermi gases [39]; however, this work assumed an intrinsic intraspecies interaction (i.e., in the Hamiltonian), while our work assumes a vanishing *bare* intraspecies interactions. The present problem of induced intraspecies interactions in imbalanced gases has previously been studied by Bulgac and collaborators [35], and by Nishida, the latter in the two-dimensional limit [40]. Additional recent work has studied the problem of polaron-polaron interactions in imbalanced Fermi gases [41], although this work did not address the possibility of p -wave pairing.

This paper is organized as follows. In Sec. II we start from the standard one-channel model Hamiltonian for imbalanced Fermi gases and develop a general Green’s-function formalism for studying intraspecies pairing in this setting. In this section we show that intraspecies pairing among the spins- \uparrow is reflected by an off-diagonal component of an associated Nambu self energy that,

in turn, depends on a matrix vertex function that we proceed to approximate in the subsequent sections. In Sec. III, we approximate this vertex function to quadratic order in perturbation theory; our results in this section are consistent with the original calculations of Kohn and Luttinger [33, 34] (who studied the general problem of induced interactions in fermions) and, more recently, Bulgac et al. [35] (who studied induced interactions in the present setting of imbalanced Fermi gases). Importantly, the perturbative formula for the transition temperature is invalid in the unitary regime where cold-atom experiments focus; in the regime where it applies, this transition temperature is orders of magnitude too small to be observable. In Sec. IV, we attempt to go beyond the perturbative limit to estimate the transition temperature for p -wave pairing among the majority species in the unitary regime. The classes of diagrams we keep for the vertex function include both ladder and crossed ladder diagrams (which, as we show, recover the conventional Fermi liquid theory of imbalanced gases), but also diagrams containing both ladder and crossed-ladder subdiagrams (the latter required to have a nonzero transition temperature). In Sec. V, we use our results from Sec. IV to estimate the magnitude of the pairing gap at the spin- \uparrow Fermi surface at $T \rightarrow 0$. In Sec. VI, we turn to the question of how the p -wave phase of imbalanced Fermi gases could be observed in radio-frequency spectroscopy and density correlation experiments before concluding in Sec. VII.

II. MODEL HAMILTONIAN AND FORMALISM

Our aim is to derive the effective interactions among one species of fermion, mediated by the other species of fermion, in a strongly imbalanced Fermi gas. In the present section we begin by developing a Green's function formalism to address this problem. Our starting point is the following one-channel model Hamiltonian for a gas of two species of fermions (labeled by $\sigma = \uparrow, \downarrow$) interacting via an s -wave Feshbach resonance [2] (note we take $\hbar = 1$):

$$H = \sum_{\sigma} \int d^3r \Psi_{\sigma}^{\dagger}(\mathbf{r}) \left[-\frac{\nabla^2}{2m} - \mu_{\sigma} \right] \Psi_{\sigma}(\mathbf{r}) + \lambda \int d^3r \hat{n}_{\uparrow}(\mathbf{r}) \hat{n}_{\downarrow}(\mathbf{r}), \quad (1)$$

where the density $\hat{n}_{\sigma}(\mathbf{r}) = \Psi_{\sigma}^{\dagger}(\mathbf{r}) \Psi_{\sigma}(\mathbf{r})$ and λ is the strength of a short-ranged pseudo-potential (approximated by a delta-function in real space). Here, μ_{σ} is the chemical potential of species σ ; the density imbalance can be considered to arise from an imbalance in the chemical potentials $\mu_{\uparrow} \neq \mu_{\downarrow}$.

The Hamiltonian Eq. (1) must be defined along with a cutoff reflecting the short-distance properties of the real physical interaction, with a corresponding scale d . Equivalently, this problem has a large momentum cutoff $\Lambda \approx 2\pi/d$ that regularizes any divergent ultraviolet (UV)

behavior coming from the singular nature of the delta-like pseudo-potential. In practice, as is well known [2], this can be handled by exchanging the bare coupling λ for the vacuum scattering length a_s that are related via

$$\frac{1}{\lambda} = \frac{m}{4\pi a_s} - \sum_{\mathbf{k}}^{\Lambda} \frac{1}{2\epsilon_{\mathbf{k}}}. \quad (2)$$

In the weak-coupling BCS limit $\lambda \rightarrow 0-$, this equation is solved by $\lambda = \frac{4\pi a_s}{m}$, i.e., we can neglect the final term on the right side of Eq. (2). In the unitary regime where a_s becomes large, we use a different procedure: If we assume physical observables are independent of Λ , then to study systems at fixed values of a_s (which is experimentally controllable) it is valid to replace λ by a_s [using Eq. (2)] in approximate theoretical expressions and then take the limit $\Lambda \rightarrow \infty$. This strategy, which is equivalent to taking $\lambda \rightarrow 0-$ and $\Lambda \rightarrow \infty$ while holding a_s fixed via Eq. (2), will naturally lead to our inclusion of certain classes of Feynman diagrams.

As we have discussed, the Kohn-Luttinger result implies that both the spin- \uparrow and spin- \downarrow Fermi surfaces of an imbalanced Fermi gas are unstable at $T \rightarrow 0$. This low- T regime, possibly consisting of two interpenetrating p -wave superfluids, is beyond the scope of this manuscript and we leave it for future work. Instead, we assume that, owing to the large population imbalance, the transition temperature for any p -wave pairing of the minority spins- \downarrow is much smaller than the corresponding temperature for the majority spins- \uparrow , as previously found in the weak-coupling BCS limit [35].

To derive the effective induced interactions among the spins- \uparrow , mediated by the spins- \downarrow , we derive self-consistent equations for the corresponding Green's functions for the two species of fermions. As discussed above, we assume the spins- \downarrow to be in an unpaired Fermi-liquid state, while the spins- \uparrow may possess pairing correlations. For the latter, accounting for such pairing correlations is best done by organizing the spin- \uparrow Green's functions using the Nambu notation:

$$\Phi_{\uparrow}(\mathbf{r}) = \begin{pmatrix} \Psi_{\uparrow}(\mathbf{r}) \\ \Psi_{\uparrow}^{\dagger}(\mathbf{r}) \end{pmatrix}. \quad (3)$$

We can then define the imaginary time ordered Nambu matrix Green's function for spins- \uparrow

$$\mathbf{G}_{\uparrow}(\mathbf{r}, \tau) = -\langle T \Phi_{\uparrow}(\mathbf{r}, \tau) \Phi_{\uparrow}^{\dagger}(0, 0) \rangle_H, \quad (4)$$

with matrix elements

$$\mathbf{G}_{\uparrow}(\mathbf{r}, \tau) = \begin{pmatrix} G_{\uparrow}(\mathbf{r}, \tau) & F_{\uparrow}(\mathbf{r}, \tau) \\ F_{\uparrow}^*(\mathbf{r}, \tau) & -G_{\uparrow}(-\mathbf{r}, -\tau) \end{pmatrix}. \quad (5)$$

The normal Green's functions are given by

$$G_{\uparrow}(\mathbf{r}, \tau) = -\langle T \Psi_{\uparrow}(\mathbf{r}, \tau) \Psi_{\uparrow}^{\dagger}(0, 0) \rangle_H, \quad (6)$$

and the anomalous ones are

$$F_{\uparrow}(\mathbf{r}, \tau) = -\langle T \Psi_{\uparrow}(\mathbf{r}, \tau) \Psi_{\uparrow}(0, 0) \rangle_H, \\ F_{\uparrow}^*(\mathbf{r}, \tau) = -\langle T \Psi_{\uparrow}^{\dagger}(\mathbf{r}, \tau) \Psi_{\uparrow}^{\dagger}(0, 0) \rangle_H. \quad (7)$$

For notational convenience, we further introduce the four-vector $k = (\mathbf{k}, i\omega_n)$. In Fourier-Matsubara space the spin- \uparrow Green's function satisfies a matrix analog of the Dyson equation

$$\mathbf{G}_\uparrow(k) = \mathbf{G}_{0,\uparrow}(k) + \mathbf{G}_{0,\uparrow}(k)\Sigma_\uparrow(k)\mathbf{G}_\uparrow(k), \quad (8)$$

where

$$\begin{aligned} \mathbf{G}_{0,\uparrow}(k) &= \begin{pmatrix} G_{0,\uparrow}(k) & 0 \\ 0 & -G_{0,\uparrow}(-k) \end{pmatrix}, \\ &= \begin{pmatrix} \frac{1}{i\omega_n - \xi_{\mathbf{k}\uparrow}} & 0 \\ 0 & \frac{1}{i\omega_n + \xi_{\mathbf{k}\uparrow}} \end{pmatrix}, \end{aligned} \quad (9)$$

with $\xi_{\mathbf{k}\sigma} = \epsilon_{\mathbf{k}} - \mu_\sigma$, and

$$\Sigma_\uparrow(k) = \begin{pmatrix} \Sigma_\uparrow(k) & \Delta_\uparrow(k) \\ \Delta_\uparrow^*(k) & -\Sigma_\uparrow(-k) \end{pmatrix}, \quad (10)$$

is the matrix self-energy. The appearance of nonzero off-diagonal terms in the self-energy indicates the presence of a superfluid state, with order parameter or gap function $\Delta_\uparrow(k)$. The self energy satisfies

$$\begin{aligned} \Sigma_\uparrow(k) &= \lambda\sigma_z \sum_q G_\downarrow(q) + \lambda\sigma_z \sum_{q,q'} \mathbf{G}_\uparrow(q)G_\downarrow(q') \times \\ &\quad \times \mathbf{\Gamma}(q, q', q + q' - k, k)G_\downarrow(q + q' - k), \end{aligned} \quad (11)$$

where σ_z is a Pauli matrix, $\mathbf{\Gamma}$ is the reducible two-particle matrix vertex function (apart from energy and momentum conserving delta functions), and the summation is $\sum_q \equiv (\beta V)^{-1} \sum_{\mathbf{q}} \sum_{i\nu_n}$, with $\beta^{-1} = k_B T$ and V the system volume (which, henceforth, we will set to unity). Diagrammatically, Eq. (11) is shown in Fig. 2.

The spin-down Green function $G_\downarrow(\mathbf{r}, \tau)$ satisfies a similar set of equations (but is assumed to be unpaired); in terms of the spin-down fermion operators it is defined as

$$G_\downarrow(\mathbf{r}, \tau) = -\langle T \Psi_\downarrow(\mathbf{r}, \tau) \Psi_\downarrow^\dagger(0, 0) \rangle_H. \quad (12)$$

Since the Green's function depends on $\Sigma_\uparrow(k)$ via the Dyson equation [Eq. (8)], this, along with Eq. (11) amount to self-consistent equations for the self-energy. For pairing to be stable, we must find a solution to these equations possessing a nonzero off-diagonal component $\Delta_\uparrow(k)$. Formally, the only assumption we have made thus far is that the spins- \downarrow are unpaired (i.e., they possess no off-diagonal component to their self energy); in practice to proceed we must make a physically-motivated approximation for the Bethe-Salpeter equation satisfied by $\mathbf{\Gamma}$.

III. LEADING-ORDER PERTURBATION THEORY

Having set up the general formalism for computing the self-consistent pairing amplitude for intraspecies pairing

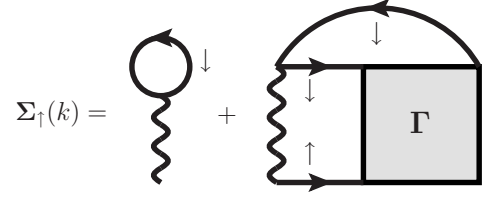


FIG. 2: The formally exact diagrammatic matrix self-energy, Eq. (11). The spin- \uparrow Green's function and vertex function $\mathbf{\Gamma}$ are Nambu matrices, while the spin- \downarrow are normal scalar functions. The interaction lines are $\lambda\sigma_z$, where σ_z is the third Pauli matrix.

correlations among the spins- \uparrow , in the present section we take the weak-coupling perturbative approximation $\lambda \rightarrow 0$ — in which these equations simplify. This will allow us to easily identify the effective interaction among the spins- \uparrow ; as we show below, a similar structure will hold when we sum diagrams to all orders in λ (to access the unitary regime). Our results in this section are consistent with those of Ref. 35.

In the weakly interacting BCS limit we can expand perturbatively in λ , or equivalently in $a_s = m\lambda/4\pi$. In fact, to obtain a nonzero result for the intraspecies pairing we must keep terms of order λ^2 . The reason for this is that, to $\mathcal{O}(\lambda)$, the self energy is simply given by the first term in Eq. (11), the Hartree contribution, $\Sigma_\uparrow(k) = \lambda\sigma_z n_\downarrow$, where n_\downarrow is the density of spins- \downarrow . At this level of approximation, the Nambu self-energy is diagonal and no pairing is induced.

To obtain results valid to quadratic order, $\mathcal{O}(\lambda^2)$, it is sufficient to approximate the vertex function by the bare interaction,

$$\mathbf{\Gamma} = -\lambda\sigma_z, \quad (13)$$

where the presence of the Pauli matrix is due to the fact that we need to write the interaction in Nambu space. This gives for the self energy:

$$\Sigma_\uparrow(k) = \lambda\sigma_z n_\downarrow - \lambda^2 \sigma_z \sum_{q,q'} \mathbf{G}_\uparrow(q)\sigma_z G_\downarrow(q')G_\downarrow(q + q' - k). \quad (14)$$

Here and in the next section (when we sum diagrams to all orders in λ), we'll neglect the diagonal component of the self-energy (simply assuming it amounts to a chemical potential shift). Within this simplifying approximation, the Green's function for the spins- \uparrow can be written as

$$\mathbf{G}_\uparrow(\mathbf{k}, i\omega_n) = \frac{1}{(i\omega_n)^2 - E_{\mathbf{k}}^2} \begin{pmatrix} i\omega_n + \xi_{\mathbf{k}\uparrow} & \Delta_\uparrow(\mathbf{k}, i\omega_n) \\ \Delta_\uparrow^*(\mathbf{k}, i\omega_n) & i\omega_n - \xi_{\mathbf{k}\uparrow} \end{pmatrix}, \quad (15)$$

where $E_{\mathbf{k}}(i\omega_n) = \sqrt{\xi_{\mathbf{k}\uparrow}^2 + \Delta_\uparrow^*(\mathbf{k}, i\omega_n)\Delta_\uparrow(\mathbf{k}, i\omega_n)}$. Comparing Eqs. (5) and (15) one can read off the relationship between the anomalous propagator and gap function

$$F_\uparrow(\mathbf{k}, i\omega_n) = -\frac{\Delta_\uparrow(\mathbf{k}, i\omega_n)}{\omega_n^2 + E_{\mathbf{k}}^2}. \quad (16)$$

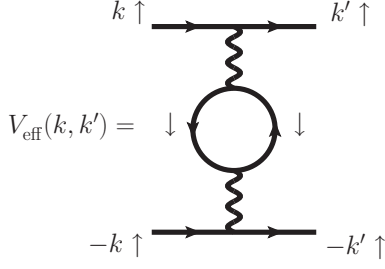


FIG. 3: The induced interaction among the spins- \uparrow , mediated by the spins- \downarrow , in the weak-coupling BCS limit. The internal loop corresponds to density fluctuations of the minority spin. The external legs are only present to label the incoming and outgoing energy and momentum.

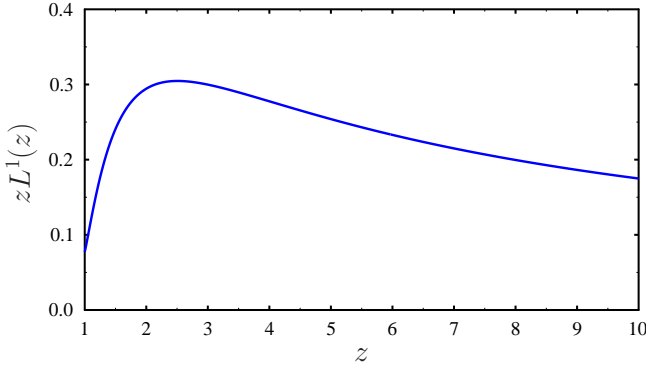


FIG. 4: (Color online) The p -wave projection of the Lindhard Function, see Eq. (20), as a function of density imbalance $z = k_{F\uparrow}/k_{F\downarrow}$. The peak near $z \approx 2$ occurs as a result as the turning off of particle-hole excitations with a transferred momentum larger than the diameter of the spin- \downarrow Fermi surface, while at smaller wave vectors the Lindhard function is approximately flat, leading to a vanishingly small p -wave projection.

This approximation also leads to a simple form for the upper-right off-diagonal component of Eq. (14):

$$\Delta_{\uparrow}(\mathbf{k}, i\omega_n) = \frac{-1}{\beta} \sum_{\mathbf{q}, i\nu_n} V_{\text{eff}}(\mathbf{k}, \mathbf{q}, i\omega_n, i\nu_n) \frac{\Delta_{\uparrow}(\mathbf{q}, i\nu_n)}{\nu_n^2 + E_{\mathbf{q}}^2}, \quad (17)$$

$$V_{\text{eff}}(k, q) \equiv \lambda^2 \sum_p G_{\downarrow}(k - q + p) G_{\downarrow}(p), \quad (18)$$

where, in the second line, we used a short hand notation $V_{\text{eff}}(k, q) \equiv V_{\text{eff}}(\mathbf{k}, \mathbf{q}, i\omega_n, i\nu_n)$. Thus, the similarity of the resulting expression to a standard gap equation for pairing has allowed us to identify an effective interaction $V_{\text{eff}}(k, k')$ that is plotted diagrammatically in Fig. III.

We proceed by approximating the full spin- \downarrow Green's function in (18) by noninteracting ones, i.e., $G_{\downarrow}(\mathbf{k}, i\omega_n) \rightarrow G_{0,\downarrow}(\mathbf{k}, i\omega_n) = (i\omega_n - \xi_{\mathbf{k}\downarrow})^{-1}$, neglecting the frequency dependence of $V_{\text{eff}}(k, k')$ (setting the Matsubara frequencies to zero), and assuming that $\Delta_{\uparrow}(\mathbf{k}, i\omega_n) = \Delta_{\uparrow}(\mathbf{k})$, i.e., it is independent of frequency.

Evaluating the remaining Matsubara sum in Eq. (17),

we arrive at the following gap equation that is of the standard form:

$$\Delta_{\uparrow}(\mathbf{k}) = - \sum_{\mathbf{q}} V_{\text{eff}}(\mathbf{k}, \mathbf{q}) \frac{\tanh(\beta E_{\mathbf{q}}/2)}{2E_{\mathbf{q}}} \Delta_{\uparrow}(\mathbf{q}), \quad (19)$$

where now the induced interactions (mediated by density fluctuations of the spins- \downarrow) are proportional to the Lindhard function:

$$V_{\text{eff}}(\mathbf{k}, \mathbf{q}) = - \left(\frac{4\pi a_s}{m} \right)^2 N_{\downarrow}(\epsilon_{F\downarrow}) L(|\mathbf{k} - \mathbf{q}|/2k_{F\downarrow}), \quad (20)$$

$$L(x) = \frac{1}{2} + \frac{1-x^2}{4x} \ln \left| \frac{1+x}{1-x} \right|, \quad (21)$$

where we have replaced $\lambda \rightarrow 4\pi a_s/m$ as noted above (valid in the weak-coupling BCS regime). Here, $k_{F\sigma}$ is the Fermi wavevector for species σ , satisfying $n_{\sigma} = \frac{k_{F\sigma}^3}{3\pi^2}$, and

$$N_{\sigma}(\epsilon_{F\sigma}) = mk_{F\sigma}/(2\pi^2), \quad (22)$$

is the density of states at the spin- σ Fermi surface.

We now decompose the gap potential and effective interaction into angular momentum channels using

$$V_{\text{eff}}(\mathbf{k}, \mathbf{k}') = \sum_{l=0}^{\infty} (2l+1) v_{k,k'}^l P_l(\hat{\mathbf{k}} \cdot \hat{\mathbf{k}}'), \quad (23)$$

$$\Delta_{\uparrow}(\mathbf{k}) = \sum_{l=0}^{\infty} (2l+1) \Delta_{k\uparrow}^l P_l(\hat{\mathbf{z}} \cdot \hat{\mathbf{k}}), \quad (24)$$

where $P_l(x)$ are the Legendre polynomials. The transition temperature for each angular momentum channel is then determined by the solution to

$$\Delta_{k\uparrow}^l = - \sum_{\mathbf{q}} v_{k,q}^l \frac{\tanh(\beta \xi_{\mathbf{q}\uparrow}/2)}{2\xi_{\mathbf{q}\uparrow}} \Delta_{q\uparrow}^l, \quad (25)$$

where we have assumed a continuous transition where the gap potential vanishes; in this limit we replace $E_{\mathbf{q}} \rightarrow \xi_{\mathbf{q}\uparrow}$. To proceed, we note that we are interested in the onset of p -wave ($l = 1$) pairing at the spin- \uparrow Fermi surface. Thus, we set $k \rightarrow k_{F\uparrow}$ in Eq. (25), and henceforth choose $l = 1$. The summation over \mathbf{q} is then dominated by the region where $q \simeq k_{F\uparrow}$. Using that the function $v_{k,q}^1$ is only nonzero for k and q within $k_{F\downarrow}$ of each other, and converting the sum to an integral (introducing the density of states), we obtain

$$\Delta_{\uparrow}^1(\epsilon_{F\uparrow}) \approx -v_{k_{F\uparrow}, k_{F\uparrow}}^1 N_{\uparrow}(\epsilon_{F\uparrow}) \int_{-\epsilon_{F\downarrow}}^{\epsilon_{F\downarrow}} d\epsilon \frac{\tanh(\beta\epsilon/2)}{2\epsilon} \Delta_{\uparrow}^1(\epsilon), \quad (26)$$

for the pairing gap near the assumed continuous transition. The corresponding transition temperature is:

$$k_B T_c \approx \frac{2\epsilon_{F\downarrow} e^{\gamma}}{\pi} \exp \left[\frac{1}{v_{k_{F\uparrow}, k_{F\uparrow}}^1 N_{\uparrow}(\epsilon_{F\uparrow})} \right], \quad (27)$$

where $\gamma = 0.577\dots$ is the Euler-Mascheroni constant, giving our result for the transition temperature expressed in terms of the $\ell = 1$ projection of the induced interactions in the weak-coupling regime $a_s \rightarrow 0^-$.

The final step in the perturbative analysis is to obtain the p -wave component of the perturbative effective interaction, Eq. (20). Then, we have for the dimensionless effective induced interaction [appearing in the argument of the exponential function of Eq. (27)] [35]:

$$v_{k_{F\uparrow}, k_{F\uparrow}}^1 N_{\uparrow}(\epsilon_{F\uparrow}) = -\frac{4(k_{F\downarrow} a_s)^2}{\pi^2} z L^1(z), \quad (28)$$

where $z = k_{F\uparrow}/k_{F\downarrow}$ and

$$L^1(z) = \frac{5z^2 - 2}{15z^4} \ln|1 - z^2| - \frac{z^2 + 5}{30z} \ln\left|\frac{1 - z}{1 + z}\right| - \frac{z^2 + 2}{15z^2}, \quad (29)$$

is the p -wave projection of the Lindhard function

$$L^1(z) = \int_0^\pi d\theta \cos\theta L(|\hat{\mathbf{k}} - \hat{\mathbf{k}}'|z/2), \quad (30)$$

with $\hat{\mathbf{k}} \cdot \hat{\mathbf{k}}' = \cos(\theta)$. The perturbative formula for T_c , given by inserting Eq. (28) into Eq. (27) thus yields a result that vanishes exponentially as $k_B T_c \exp[-c/(k_F a_s)^2]$ with $c > 0$; if this estimate is correct, then such p -wave pairing is probably not experimentally observable in the weak-coupling perturbative regime.

For fixed $k_{F\downarrow} a_s$, the density imbalance dependence enters through $z L^1(z)$, that we plot in Fig. 4. We see that this quantity shows a maximum value near $z \approx 2$, leading to a peak in the p -wave transition temperature near a polarization of $P \approx 0.77$; we find a similar peak in T_c in our unitary-regime results to follow.

In the next section we proceed to derive a formula for T_c which goes beyond the weak-coupling regime. Our result is of the same form as Eq. (27) but with a more complicated expression for the effective induced interactions $v_{k_{F\uparrow}, k_{F\uparrow}}^1$, including contributions from all orders of λ . Our final result for T_c in fact reduces to the perturbative result of this section when we take the weak-coupling limit $a_s \rightarrow 0^-$; however, in the regime where they agree (far to the right of the displayed area of Fig. 8), T_c is many orders of magnitude smaller than the maximum transition temperature shown in Fig. 1.

IV. BEYOND LEADING ORDER

In the preceding section, we showed that, within leading-order perturbation theory, there is a transition to a p -wave superfluid of the majority species of a population-imbalanced Fermi gas, although the predicted perturbative temperature is vanishingly small. In the present section, we show how additional classes of diagrams, occurring near the unitary regime, can lead to an enhanced T_c . To investigate the induced interaction in

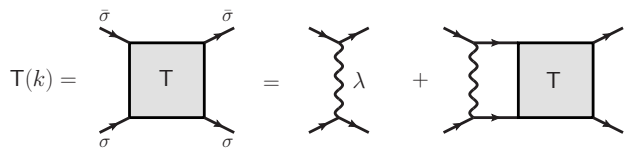


FIG. 5: The T-matrix, which describes the ladder sum of two particles interacting through the bare potential infinitely many times. Here, the solid lines are Greens functions and the wavy line is the interaction λ .

the strongly interacting regime, near unitarity, one must sum an infinite number of diagrams, to all orders of the bare interaction λ , contributing to the Nambu self-energy Eq. (11). We begin with the conventional T-matrix approximation, which, when extended to a system with pairing correlations, includes ladder and crossed-ladder diagrams.

A. Ladder plus crossed ladder approximation

Recent work has found that the nonsuperfluid Fermi liquid phase of imbalanced Fermi gases is well described by the so-called T-matrix approximation for the self-energy or more specifically for the vertex [26, 27, 32], depicted diagrammatically in Fig. 5. In the case of unpaired spins- \uparrow , this approximation amounts to summing the repeated interaction of a spin- \uparrow particle with a single spin- \downarrow particle-hole bubble, as shown diagrammatically in the self energy shown in Fig. 6(a).

Our aim is to generalize the T-matrix approximation to imbalanced Fermi gases by including the possibility of pairing for the spins- \uparrow . The simplest way to do this is to keep the same series of diagrams, but replace the normal Green's function $G_{\uparrow}(k)$ with the corresponding Nambu Green's function, i.e., considering the same ladder series but with $G_{\uparrow}(k) \rightarrow \mathbf{G}_{\uparrow}(k)$. We refer to this Nambu T-matrix with the bold symbol $\mathbf{T}(k)$. Formally it is the same as Fig. 5 but with the spin- \uparrow Green's functions possessing Nambu structure (while the spin- \downarrow Green's function is still a normal Green's function); additionally the coupling (wavy line) is given by $\lambda \sigma_z$. The corresponding self energy is given in Fig. 6(a).

However, this ladder series is not sufficient for our purposes, as can be seen by noting that it does not even reproduce the standard T-matrix approximation in the limit $\Delta_{\uparrow}(k) \rightarrow 0$. This is because, in the Nambu notation, the lower right element of Eq. (5) can be regarded as a Green's function with a line possessing opposite momentum from the upper left element, i.e., its momentum is in the opposite direction. This means that, in addition to ladder diagrams, we must include maximally-crossed diagrams shown in Fig. 6(d).

The conclusion of the preceding remarks is that the set of diagrams needed to minimally generalize the usual T-matrix approximation to a system with pairing among

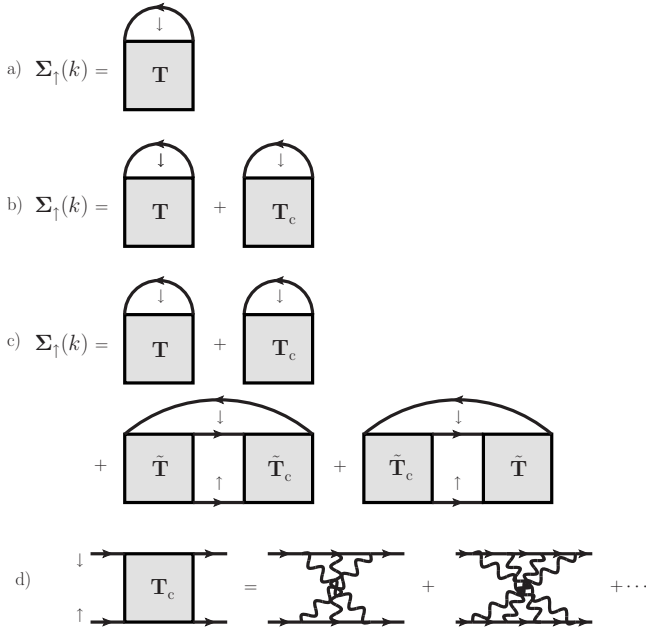


FIG. 6: The diagrammatic contributions of the spin- \uparrow Nambu self-energy at various levels of approximations. Where \mathbf{T} , defined by Eq. (32), corresponds to the Nambu matrix generalization of the \mathbf{T} -matrix, shown in Fig. 5, where all spin- \uparrow Green's functions are in Nambu space while the spins- \downarrow are scalar functions and interaction lines correspond to $\lambda\sigma_z$. Here \mathbf{T}_c , given by Eq. (33), is the Nambu generalized, sum of the so-called maximally crossed diagrams, shown in panel d, $\tilde{\mathbf{T}} = \mathbf{\Pi}_A \mathbf{T}$ and $\tilde{\mathbf{T}}_c = -\mathbf{\Pi}_B^{-1} \mathbf{T}_c$, with $\mathbf{\Pi}_A$ and $\mathbf{\Pi}_B$ defined by Eq. (34) and Eq.(35) respectively.

the spins- \uparrow is given by Fig. 6(b). The first term contains the ladder series and the second term contains the crossed diagrams Fig. 6(d). This gives:

$$\Sigma_{\uparrow}(k) = \sum_q \mathbf{T}(k+q)G_{\downarrow}(q) + \sum_q \mathbf{T}_c(q-k)G_{\downarrow}(q), \quad (31)$$

where

$$\mathbf{T}(k) = \sigma_z [\mathbb{1}\lambda^{-1} + \mathbf{\Pi}_A(k)]^{-1}, \quad (32)$$

$$\mathbf{T}_c(k) = \lambda^2 \sigma_z \mathbf{\Pi}_B^2(k) [\mathbb{1}\lambda^{-1} + \mathbf{\Pi}_B(k)]^{-1} \quad (33)$$

Here, the inverse is understood as a matrix inverse and the bubbles $\mathbf{\Pi}_A(k)$ and $\mathbf{\Pi}_B(k)$ are given by

$$\mathbf{\Pi}_A(k) = \sum_q \mathbf{G}_{\uparrow}(q)G_{\downarrow}(k-q)\sigma_z, \quad (34)$$

$$\mathbf{\Pi}_B(k) = \sum_q \mathbf{G}_{\uparrow}(q)G_{\downarrow}(k+q)\sigma_z. \quad (35)$$

Having derived the natural generalization of the ladder approximation to incorporate the possibility of intraspecies pairing among the spins- \uparrow , we now show that, in the unitary regime, it cannot possess any off-diagonal pairing correlations but merely reproduces the polaron

Fermi liquid, implying that we must go beyond this level of approximation. To do this, we make the replacement Eq. (2) and take the limit $\Lambda \rightarrow \infty$ while holding a_s fixed (a procedure that, above, we argued to be valid away from the weak-coupling BCS limit). The Nambu \mathbf{T} -matrix is thus

$$\mathbf{T}(k) = \sigma_z \left[\mathbb{1} \frac{4\pi a_s}{m} + \mathbf{\Pi}_A(k) - \mathbb{1} \sum_{\mathbf{k}}^{\Lambda} \frac{1}{2\epsilon_{\mathbf{k}}} \right]^{-1}, \quad (36)$$

where, when we take the limit $\Lambda \rightarrow \infty$, it is clear that the last term yields a divergence proportional to the identity matrix. To be nonzero, a similar divergence must appear in $\mathbf{\Pi}_A(k)$; however, because of the Nambu structure of $\mathbf{G}_{\uparrow}(q)$, only the upper left component of $\mathbf{\Pi}_A$ can possess such a divergence. Thus, all elements of $\mathbf{T}(k)$ except the upper-left will vanish, and we obtain:

$$\lim_{\Lambda \rightarrow \infty} \mathbf{T}(k) = \begin{pmatrix} \mathbf{T}(k) & 0 \\ 0 & 0 \end{pmatrix}, \quad (37)$$

where $\mathbf{T}(k)$ is the usual \mathbf{T} -matrix, satisfying

$$\begin{aligned} [\mathbf{T}(\mathbf{k}, i\nu_n)]^{-1} &= \frac{4\pi a_s}{m} \\ &+ \frac{1}{\beta} \sum_{\mathbf{q}, i\nu_n} G_{\uparrow}(\mathbf{q}, i\nu_n) G_{\downarrow}(\mathbf{k} - \mathbf{q}, i\nu_n - i\nu_n) - \sum_{\mathbf{q}} \frac{1}{2\epsilon_{\mathbf{q}}}. \end{aligned} \quad (38)$$

To be clear, the quantity $G_{\uparrow}(\mathbf{q}, i\nu_n)$ appearing in this formula is the upper-left component of the full matrix Green's function $\mathbf{G}_{\uparrow}(\mathbf{q}, i\nu_n)$. A similar simplification occurs in $\mathbf{T}_c(k)$, which, when we make the same replacement and take the limit of $\Lambda \rightarrow \infty$, yields

$$\lim_{\Lambda \rightarrow \infty} \mathbf{T}_c(k) = \begin{pmatrix} 0 & 0 \\ 0 & -\mathbf{T}(-k) \end{pmatrix}, \quad (39)$$

giving for the self-energy

$$\Sigma_{\uparrow}(k) = \sum_q \begin{pmatrix} \mathbf{T}(q+k) & 0 \\ 0 & -\mathbf{T}(q-k) \end{pmatrix} G_{\downarrow}(q), \quad (40)$$

which, crucially is *diagonal* in Nambu space and, thus, possesses no pairing correlations. In fact, Eq. (40) is exactly the self-energy within the usual “polaron” Fermi liquid description of strongly imbalanced Fermi gases, equivalent to the Chevy variational wavefunction [30] as shown in Ref. 31.

Thus, although we generalized the ladder approximation in the simplest possible way to include pairing correlations (summing ladder and crossed-ladder diagrams but with a *Nambu* spin- \uparrow Green's function), we have found that, within this approximation, such pairing correlations are not stable. The results of this section, however, tell us two things: Firstly, we must consider sets of diagrams that go beyond this approximation. Secondly, to have a result that is finite when we make the replacement Eq. (2) and take $\Lambda \rightarrow \infty$, we must consider diagrams with ladder or crossed-ladder type subdiagrams.

B. Combined ladder and crossed-ladder diagrams

As we have seen, the ladder and crossed-ladder (or maximally-crossed) sets of diagrams contain geometric sums that are nonzero when we exchange the bare coupling λ for the scattering length a_s using Eq. (2) and take the limit $\Lambda \rightarrow \infty$. Since the quantities $\mathbf{T}(k)$ and $\mathbf{T}_c(k)$ are diagonal in this limit, each possessing only one nonzero element, the corresponding contributions to the self-energy in Fig. 6(b) are also diagonal. However, there exist additional sets of diagrams containing $\mathbf{T}(k)$ and $\mathbf{T}_c(k)$ as subdiagrams that are *not* diagonal in this limit; the simplest such self-energy diagrams are shown as the final two diagrams in Fig. 6(c). Our inclu-

sion of these diagrams may alternatively be understood on physical grounds as due to the fact that paired superfluidity mixes particles and holes: roughly speaking, \mathbf{T} describes particle-particle scattering and \mathbf{T}_c describes hole-hole scattering. Including pairing requires mixing these, suggesting the incorporation of these diagrams. Thus, Fig. 6(c) represents the full set of self-energy diagrams that we consider here: The ladder and crossed-ladder terms that yield the polaron Fermi liquid (as shown above) and the combined ladder and crossed-ladder diagrams that, as we now show, capture the instability of the polaron Fermi liquid to p -wave pairing. This self energy is:

$$\begin{aligned} \Sigma_{\uparrow}(k) = & \sum_q \mathbf{T}(k+q)G_{\downarrow}(q) + \sum_q \mathbf{T}_c(q-k)G_{\downarrow}(q) \\ & - \lambda^2 \sigma_z \sum_{q,q'} \mathbf{\Pi}_A(k+q) [\mathbb{1}\lambda^{-1} + \mathbf{\Pi}_A(k+q)]^{-1} \mathbf{G}_{\uparrow}(q) \sigma_z \mathbf{\Pi}_B(q'-q) [\mathbb{1}\lambda^{-1} + \mathbf{\Pi}_B(q'-q)]^{-1} G_{\downarrow}(q'-q+k)G_{\downarrow}(q') \\ & - \lambda^2 \sigma_z \sum_{q,q'} \mathbf{\Pi}_B(q'-k) [\mathbb{1}\lambda^{-1} + \mathbf{\Pi}_A(q'-k)]^{-1} \mathbf{G}_{\uparrow}(q) \sigma_z \mathbf{\Pi}_A(q+q') [\mathbb{1}\lambda^{-1} + \mathbf{\Pi}_A(q+q')]^{-1} G_{\downarrow}(q+q'-k)G_{\downarrow}(q'). \end{aligned} \quad (41)$$

Again exchanging λ for a_s using Eq. (2) and letting $\Lambda \rightarrow \infty$, we get

$$\lambda \sigma_z \mathbf{\Pi}_A(k) [\mathbb{1}\lambda^{-1} + \mathbf{\Pi}_A(k)]^{-1} \rightarrow \begin{pmatrix} \mathbf{T}(k) & 0 \\ 0 & 0 \end{pmatrix} \quad (42)$$

and

$$\lambda \sigma_z \mathbf{\Pi}_B(k) [\mathbb{1}\lambda^{-1} + \mathbf{\Pi}_B(k)]^{-1} \rightarrow \begin{pmatrix} 0 & 0 \\ 0 & -\mathbf{T}(k) \end{pmatrix}, \quad (43)$$

so that Eq. (41) reduces to

$$\Sigma_{\uparrow}(k) = \sum_q \begin{pmatrix} \mathbf{T}(q+k)G_{\downarrow}(q) & V_{\text{eff}}(k,q)F_{\uparrow}(q) \\ V_{\text{eff}}(k,q)F_{\uparrow}^*(q) & -\mathbf{T}(q-k)G_{\downarrow}(q) \end{pmatrix}, \quad (44)$$

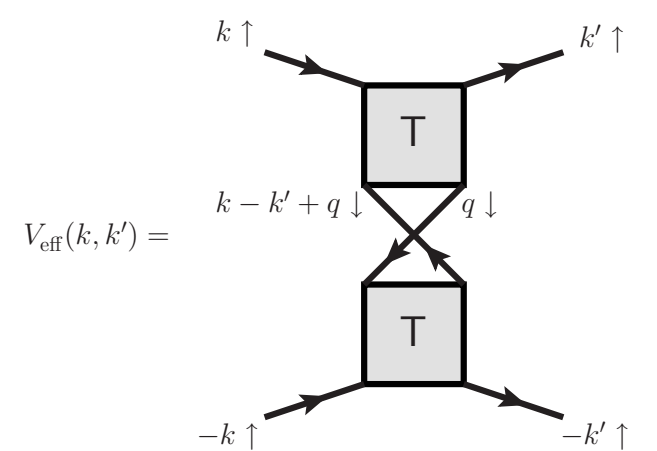
where the effective pairing interaction $V_{\text{eff}}(k, k')$ is shown diagrammatically in Fig. 7 and is explicitly given by

$$V_{\text{eff}}(k, k') = \sum_q \mathbf{T}(q+k)\mathbf{T}(q-k')G_{\downarrow}(k-k'+q)G_{\downarrow}(q). \quad (45)$$

The effective interaction Eq. (45) is a direct generalization of the induced interaction of the weak BCS limit (18), except now with a energy and momentum dependent coupling, i.e., the bare interaction λ in Eq. (18) has been replaced by the \mathbf{T} -matrix in Eq. (45).

With this effective interaction, the gap equation is

$$\Delta_{\uparrow}(k) = \sum_q V_{\text{eff}}(k, q)F_{\uparrow}(q), \quad (46)$$



problem simplifies near the assumed continuous phase transition, where $\Delta_{\uparrow}(\mathbf{k})$ vanishes, a regime we now focus on. In this regime, we can simply approximate the T matrices by their form in the imbalanced normal phase.

In principle all of the Green's functions appearing in the effective interaction Eq. (45) are the exact interacting Green's functions. To proceed, we make some simplifying approximations, firstly by replacing these with their noninteracting expressions (equivalent to assuming the imbalanced Fermi liquid phase is noninteracting) and neglecting the external frequency dependence of Eq. (45) (i.e., setting $\omega_k = \omega'_k \rightarrow 0$). This gives

$$V_{\text{eff}}(\mathbf{k}, \mathbf{k}') = 2T \sum_{\Omega} \int \frac{d^3q}{(2\pi)^3} T(\mathbf{q} + \mathbf{k}, i\Omega) T(\mathbf{q} - \mathbf{k}', i\Omega) \times \frac{1}{i\Omega - \xi_{\mathbf{k}-\mathbf{k}'+\mathbf{q}\downarrow}} \frac{1}{i\Omega - \xi_{\mathbf{q}\downarrow}}. \quad (47)$$

The sum over Matsubara frequencies can be evaluated using the standard trick [44] that requires the location of the poles of the summand in the complex plane. This is simplified by our knowledge that poles of the normal-state T -matrix on the real axis occur at the onset of s -wave paired superfluidity. Since we are studying the strongly imbalanced limit, we can assume no such poles contribute, and proceed by keeping only the poles from the Green's functions in the second line of Eq. (47). This leads to

$$V_{\text{eff}}(\mathbf{k}, \mathbf{k}') = 2T \sum_{\Omega} \int \frac{d^3q}{(2\pi)^3} T(\mathbf{q} + \mathbf{k}, \xi_{\mathbf{q}\downarrow}) T(\mathbf{q} - \mathbf{k}', \xi_{\mathbf{q}\downarrow}) \times \frac{n_F(\xi_{\mathbf{q}\downarrow})}{\epsilon_q - \epsilon_{\mathbf{k}-\mathbf{k}'+\mathbf{q}}}, \quad (48)$$

our final result for the static induced interaction for the majority spins- \uparrow , mediated by the spins- \downarrow , in a strongly interacting imbalanced Fermi gas.

Our main results come from numerically evaluating Eq. (48). However, it is useful to first make a bit more approximate analytic progress by invoking an approximation that is valid in the large-imbalance limit. Thus, to evaluate the remaining integral over \mathbf{q} , we begin by noting that the Fermi function restricts, at low T , the momentum to $q < k_{F\downarrow}$, inside the spin- \downarrow Fermi surface. But since we're interested in the regime where \mathbf{k} and \mathbf{k}' are on the spin- \uparrow Fermi surface, in the strongly imbalanced limit $k_{F\uparrow} \gg k_{F\downarrow}$ the momentum argument of the T -matrices in Eq. (48) is approximately given simply by $k_{F\uparrow}$. In this strongly imbalanced limit the first T -matrix in Eq. (48) simplifies to

$$T(\mathbf{k}_F, \xi_{\mathbf{q}\downarrow}) \simeq \left(\frac{m}{4\pi a_s} - \frac{mk_{F\uparrow}}{4\pi^2} \right)^{-1}, \quad (49)$$

with a similar expression holding for the second T -matrix in Eq. (48). Within this approximation, valid at large population imbalance $P \rightarrow 1$, the T -matrices are thus independent of momenta. As can be seen in the original expression Eq. (44), when this occurs V_{eff} is simply

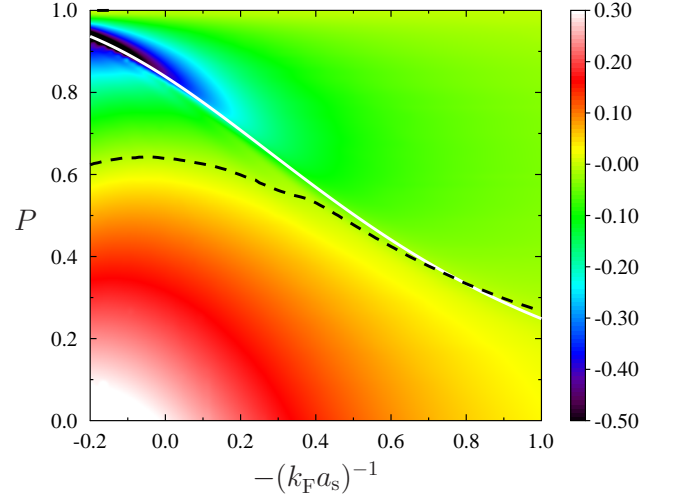


FIG. 8: (Color online) The p -wave channel of the effective interaction between majority spins, $v_{k_{F\uparrow}, k_{F\uparrow}}^1$, multiplied by the Fermi-energy density of states $N_{\uparrow}(\epsilon_{F\uparrow})$, as a function of the density imbalance P and s -wave scattering length a_s , is shown. Here, $k_F = (k_{F\uparrow} + k_{F\downarrow})/2$. At large P , above the dashed line, it is *attractive* leading to a p -wave superfluid at temperatures below T_c . The solid white line labels the location of a line of FFLO quantum critical points, defined by $T(\mathbf{Q}_{\text{FFLO}}, 0) \rightarrow \infty$, at zero temperature. This coincides with the location where $v_{k_{F\uparrow}, k_{F\uparrow}}^1$ is large.

proportional to the bare bubble occurring in the weakly interacting regime (see Eq. (18)). Evaluating the remaining integrals and making the projection to the p -wave channel (as we did in the weakly interacting regime), we obtain

$$k_B T_c \approx \frac{2e^\gamma}{\pi} \epsilon_{F\downarrow} \exp \left[-\frac{3}{2} \frac{z}{\ln(z)} \left(\frac{\pi}{2k_{F\downarrow} a_s} - \frac{z}{2} \right)^2 \right], \quad (50)$$

with $z = k_{F\uparrow}/k_{F\downarrow}$, a result that we emphasize is only valid in the asymptotic strongly imbalanced regime.

Away from this $P \rightarrow 1$ limit, we must perform a numerical evaluation of the integral in Eq. (48) and the p -wave projection; this yields a dimensionless effective interaction $v_{k_{F\uparrow}, k_{F\uparrow}}^1 N_{\uparrow}(\epsilon_{F\uparrow})$ that we plot in Fig. 8 and in the top panel of Fig. 10. For this calculation we assumed the $T \rightarrow 0$ limit; since our resulting transition temperature is still small compared to the spin- \uparrow Fermi energy this should be an accurate approximation. These figures show that we find attractive interactions in the p -wave channel over a wide range of the interactions and the population imbalance.

The corresponding transition temperature, plotted in the bottom panel of Fig. 10 as well as in the phase diagram Fig. 1, is given by the same formula as in the weak-coupling limit, i.e.,

$$k_B T_c \approx \frac{2\epsilon_{F\downarrow} e^\gamma}{\pi} \exp \left[\frac{1}{v_{k_{F\uparrow}, k_{F\uparrow}}^1 N_{\uparrow}(\epsilon_{F\uparrow})} \right], \quad (51)$$

where to arrive at this formula we used the fact that, as in the weak-coupling limit, $v_{k,k'}^1$ (the p -wave projection of Eq. (48)) is only nonzero for k and k' close to each other, within a window of approximately $\pm\epsilon_{F\downarrow}$. We have verified this numerically; a plot displaying the typical behavior of $v_{k,k'}^1$ is shown in Fig. 9.

It is interesting to compare the value of T_c obtained via a direct numerical evaluation of Eq. (48) to our approximate asymptotic formula Eq. (50). In Fig. 11 we plot these as a function of population imbalance for three different values of the scattering length. These curves show that, while Eq. (50) is accurate asymptotically close to $P = 1$, it misses the peak and drop in T_c that generically occurs with decreasing P .

What is the origin of this peak in the predicted T_c occurring for very large imbalance? Certainly, one expects an increase in T_c as P decreases from unity, arising from the increase in the density of spins- \downarrow which provide the induced interactions. More precisely, the effective interactions among the spins- \uparrow are mediated by particle-hole excitations of the spins- \downarrow . However, particle-hole excitations with a wavevector larger than the diameter of the spin-down Fermi surface ($2k_{F\downarrow}$) are energetically suppressed, implying that the density response function is strongly varying for $k \simeq 2k_{F\downarrow}$. This strong variation as a function of momentum leads to a large p -wave projection of the induced interaction when $k \simeq k_{F\downarrow}$ (since, for p -wave pairing, we require an attractive interaction that strongly varies around the spin- \uparrow Fermi surface). If we then assume that the maximum T_c will occur when $k_{F\uparrow} = 2k_{F\downarrow}$, we are led to the prediction that T_c will peak near

$$P = \frac{k_{F\uparrow}^3 - k_{F\downarrow}^3}{k_{F\uparrow}^3 + k_{F\downarrow}^3} = \frac{7}{9} \simeq 0.78, \quad (52)$$

close to the value of the peak position shown in Fig. 10.

We note that Eq. (52) only *approximately* locates the peak position; indeed, Fig. 10 shows some variation of the peak position as a function of interactions. (We have not pushed this computation deep into the BEC regime where we know the magnetic superfluid ground state intervenes [12, 15].) Indeed, the preceding argument is strictly true in the weak-coupling limit where the effective interaction is given by the Lindhard function $L(x)$ that has a singularity near $x = 1$ that leads to a similar peak in T_c in the weak coupling limit. (Although, as mentioned above, the weak-coupling T_c is orders of magnitude smaller than the values plotted here.) In the strong-coupling limit, we expect this argument to still approximately hold since there the Luttinger theorem ensures that the presence of spin- \uparrow and spin- \downarrow Fermi surfaces at the same volume as in the weakly interacting limit (until the broken symmetry phase appears) [45, 46].

We also note an additional possible reason for the occurrence of a peak in T_c at large imbalance: A proximate FFLO instability. Thus, one expects an instability towards FFLO pairing for imbalanced Fermi gases, occurring when there is a divergence of the retarded T matrix at

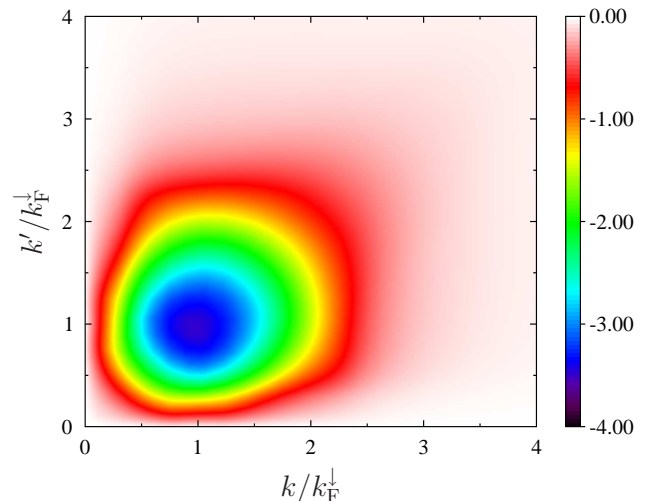


FIG. 9: (Color online) The momentum dependence of the p -wave channel $v_{k,k'}^1$ of the effective interaction, Eq. (45), as defined by Eq. (23), for zero frequency and at unitarity for a polarization of $P = 0.85$. As one can see the interaction is nonzero only within a window of approximately $k = k' \pm k_{F\downarrow}$.

zero frequency (but nonzero wavevector \mathbf{Q}_{FFLO}). In the vicinity of such a phase transition, the T matrix would, correspondingly, possess a large magnitude that would enhance the effective induced interactions. To test this, in Fig. 8, we plot, as a white line, the P at which such a *zero temperature* FFLO instability would first occur; as seen in this plot it closely correlates to the regime where the p -wave T_c is largest. Our calculation of this FFLO transition of course neglected the possibility of p -wave pairing among the spins- \uparrow . Thus, if the p -wave transition occurs first, with decreasing temperature, it would likely move the location of the FFLO phase boundary. Further detailed analysis will be required to sort out these various competing instabilities.

We conclude this section by briefly justifying the use of the on-shell approximation, in which we assume that we only need the p -wave induced interactions for momenta on the spin- \uparrow Fermi surface. As is known from the theory of superconductivity, such an approximation is typically only valid for weakly interacting quasiparticles and, near unitarity, particles of opposite spin are strongly interacting. Despite this, in highly imbalanced systems the lifetime of the quasiparticles remains extremely long; this implies the quasiparticle-quasiparticle interaction is still quite weak. This can be seen directly from the experimental and theoretical results of Ref. [28]. In Ref. [28] the Fermi liquid properties of systems with an imbalance as low as $P \approx 0.70$ were explained well within a theoretical framework consisting of only a single spin- \downarrow quasiparticle, which indicates induced interactions of like spins, is subdominant to such things as the renormalization of the chemical potential and effective mass, at least for $T \gtrsim T_c$.

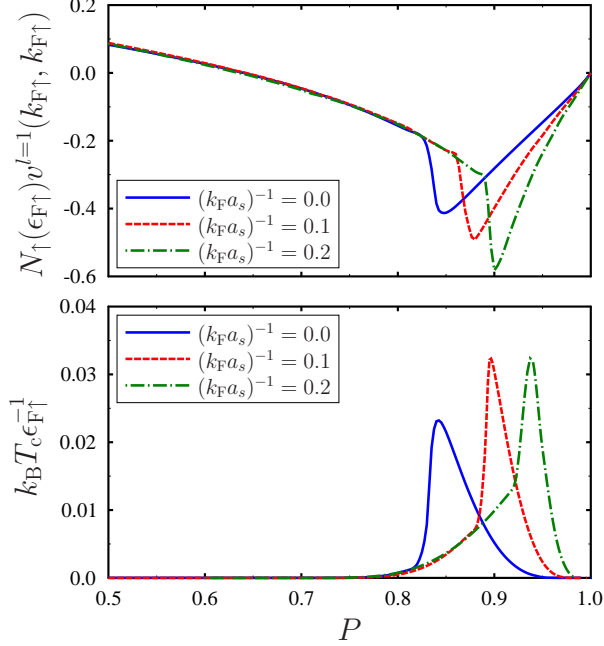


FIG. 10: (Color online) The top panel shows the on-shell $\ell = 1$ channel of the effective interaction (45) for spin- \uparrow fermions, times the density of states, as a function of polarization, at unitary and into the BEC side. The bottom panel shows the corresponding p -wave transition temperature, according to Eq. (27), with $\epsilon_{F\uparrow}/\epsilon_{F\downarrow} = [(1+P)/(1-P)]^{2/3}$.

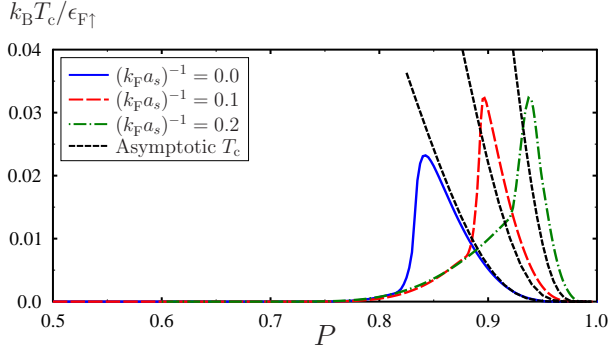


FIG. 11: (Color online) A comparison of the transition temperature obtained from Eq. (50), valid for asymptotically large polarizations, and a full numerical treatment of the induced interaction Eq. (45), using Eq. (51), with $\epsilon_{F\uparrow}/\epsilon_{F\downarrow} = [(1+P)/(1-P)]^{2/3}$.

Thus, we argue that our analysis is valid if the strongly imbalanced nonsuperfluid phase is truly a Fermi liquid for $T \gtrsim T_c$.

V. LOW-TEMPERATURE PAIRING GAP

In the present section our goal is to estimate the magnitude of the p -wave pairing gap at $T \rightarrow 0$. One subtlety is that our method for calculating the induced attraction among the spins- \uparrow is only valid for $T > T_c$, since we neglect the pairing among the spins- \uparrow in computing the T matrix. However, if we assume that the induced pairing $\Delta_{\uparrow}(\mathbf{k})$ is small in magnitude compared to $\epsilon_{F\uparrow}$ (as one might expect), then we can assume $\Delta_{\uparrow}(\mathbf{k})$ has only a small effect on the T matrix, and proceed to neglect it when estimating $\Delta_{\uparrow}(\mathbf{k})$.

The relevant equation for the low-temperature gap is Eq. (19), but with $V_{\text{eff}}(\mathbf{k}, \mathbf{q})$ given by Eq. (48). Focusing on the p -wave channel, we have, for $T \rightarrow 0$,

$$\Delta_{\uparrow}(\mathbf{k}) = -3 \sum_{\mathbf{q}} v_{k,q}^1 \hat{k} \cdot \hat{q} \frac{\Delta_{\uparrow}(\mathbf{q})}{2E_{\mathbf{q}}}. \quad (53)$$

Following the work of Anderson and Morel, we expect the dominant p -wave instability to be of the $p_x + ip_y$ form [47]. We thus write

$$\Delta_{\uparrow}(\mathbf{k}) = \Delta(k^2)(\hat{k}_x + i\hat{k}_y). \quad (54)$$

Converting the sum in Eq. (53) to an integral (recall we set the system volume to unity), we obtain

$$\Delta(k^2) = -\frac{3}{16\pi^2} \int_0^\infty q^2 dq \Delta(q^2) v_{k,q}^1 \frac{1}{|\xi_{q\uparrow}|} F\left[\frac{|\xi_{q\uparrow}|}{\Delta(q^2)}\right], \quad (55)$$

where the function

$$F[x] \equiv x^2 \left[1 + x \left(\frac{1}{x^2} - 1 \right) \tan^{-1} \frac{1}{x} \right], \quad (56)$$

arises from evaluating the angular integration. We now use the fact that $v_{k,q}^1$ is sharply peaked near $k = q$, and assume the rest of the integrand of Eq. (55) is smooth there. This yields the approximate formula

$$1 \simeq -\frac{3}{16\pi^2} \bar{v}_k \frac{k^2}{|\xi_{k\uparrow}|} F_1\left[\frac{|\xi_{k\uparrow}|}{\Delta(k^2)}\right], \quad (57)$$

$$\bar{v}_k \equiv \int_0^\infty dq v_{k,q}^1. \quad (58)$$

Restricting attention to the vicinity of the Fermi surface by setting $k \rightarrow k_{F\uparrow}$, and using the asymptotic value of $F[x] \rightarrow \frac{\pi}{2}x$ for $x \rightarrow 0$, we have

$$\Delta(k_{F\uparrow}^2) \simeq -\frac{3}{32\pi} \bar{v}_{k_{F\uparrow}} k_{F\uparrow}^2. \quad (59)$$

We can further simplify this formula by noting that, since $v_{k,q}^1$ is peaked for $k = q$ with a width of approximately $\pm k_{F\downarrow}$, we have $\bar{v}_{k_{F\uparrow}} \simeq 2k_{F\downarrow} v_{k_{F\uparrow}, k_{F\uparrow}}^1$. Then, normalizing $\Delta(k_F^2)$ to the Fermi energy and using Eq. (22), we have

$$\frac{\Delta(k_F^2)}{\epsilon_{F\uparrow}} \simeq -\frac{3\pi}{4} \frac{k_{F\downarrow}}{k_{F\uparrow}} N_{\uparrow}(\epsilon_{F\uparrow}) v^1(k_{F\uparrow}, k_{F\uparrow}). \quad (60)$$

The product of the last two factors of Eq. (60) is precisely what is plotted in Fig. 10. At unitarity, $a_s^{-1} = 0$, this factor reaches $\simeq 0.4$ at $P \simeq 0.85$, or $\frac{k_{F\downarrow}}{k_{F\uparrow}} \simeq 0.43$. Plugging these values into Eq. (60) gives the estimate $\frac{\Delta(k_F^2)}{\epsilon_{F\uparrow}} \approx 0.4$. Although this estimate is rather large, it is important to keep in mind that this is the maximum pairing gap; the full gap function will exhibit nodes according to Eq. (54). An important issue for future work is to find a more accurate estimate for the low- T pairing gap for the majority species of an imbalanced Fermi gas.

VI. EXPERIMENTAL DETECTION

We argue that, although small (a few percent of the Fermi energy), the transition temperature is within range of current experimental capabilities [55]. However, the experimental detection of such a state may still be challenging. One striking way to identify the presence of superfluidity is via the presence of vortices in a rapidly-rotating cloud, as done in Ref. 51 to detect s -wave pairing correlations. However, in Ref. 51 the detection of BCS pairs was accomplished by ramping the magnetic field onto the BEC side of the resonance, changing them into molecular pairs. For the case of the p -wave Cooper pairs predicted here, it is not clear that such a ramp is possible.

Owing to this difficulty, here we focus on two other possible ways to detect $p_x + ip_y$ Cooper pairing among the majority species of an imbalanced Fermi gas: Radio-Frequency (RF) spectroscopy (in which pairing correlations are detected by a shift in the rate at which atoms in a particular state are transferred to a third unoccupied level [48]) and noise correlations (studied theoretically in Ref. 49 and experimentally in Ref. 50).

A. RF spectroscopy of the majority spin p -wave superfluid

To use RF spectroscopy to probe $p_x + ip_y$ pairing of the spins- \uparrow , one would measure the number of spin- \uparrow atoms transferred to a known unoccupied level, as a function of applied RF frequency [53]. Neglecting final state effects, the total transferred at a given frequency is given by

$$I_\sigma(\omega) \propto \sum_{\mathbf{k}} A_\sigma(\mathbf{k}, \xi_{\mathbf{k}\sigma} - \omega) n_F(\xi_{\mathbf{k}\sigma} - \omega), \quad (61)$$

where the spectral function $A_\sigma(k)$ is related to the imaginary part of the retarded Green's function $G_\sigma^r(k)$ by

$$A_\sigma(k) = -\frac{1}{\pi} \text{Im} G_\sigma^r(k), \quad (62)$$

and $n_F(\omega)$ is the Fermi distribution function. It is convenient to write the superfluid Green's function in the mean-field spectral representation:

$$G_\uparrow^r(\mathbf{k}, \omega) = \frac{u_{\mathbf{k}}^2}{\omega - E_{\mathbf{k}} + i\eta} + \frac{v_{\mathbf{k}}^2}{\omega + E_{\mathbf{k}} + i\eta}, \quad (63)$$

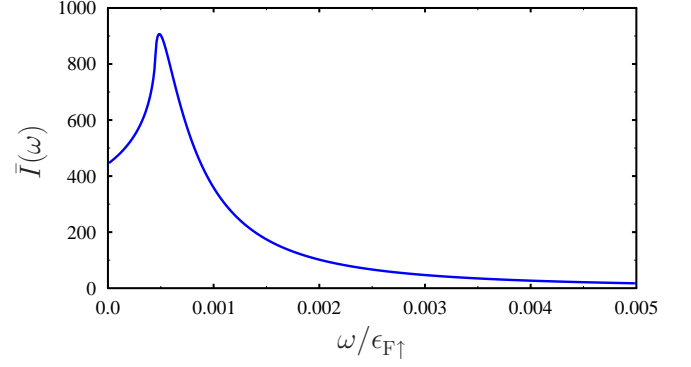


FIG. 12: (Color online) The normalized zero temperature RF line-shape (61), $\bar{I}(\omega) = I_\uparrow(\omega)/\int_0^\infty d\omega I_\uparrow(\omega)$, of a p -wave superfluid, with a $p_x + ip_y$ ground state. The magnitude of the gap is approximated by the transition temperature, $\Delta_0 \approx 0.03\epsilon_{F\uparrow}$ and the chemical potential $\mu_\uparrow \approx \epsilon_{F\uparrow}$, for $P \approx 0.85$ at unitarity. In general for a $p_x + ip_y$ ground state the peak occurs near $\omega \simeq \sqrt{\mu_\uparrow^2 + \Delta_0^2} - \mu_\uparrow$, and as $\omega \rightarrow \infty$, $\bar{I}(\omega) \rightarrow \omega^{-3/2}$, while for $\omega \rightarrow 0$, $\bar{I}(\omega) \rightarrow (\omega + 2\mu_\uparrow)^{5/2}$.

where the so-called coherence factors are

$$\begin{aligned} u_{\mathbf{k}}^2 &= \frac{1}{2} \left(1 + \frac{\xi_{\mathbf{k}\uparrow}}{E_{\mathbf{k}}} \right), \\ v_{\mathbf{k}}^2 &= \frac{1}{2} \left(1 - \frac{\xi_{\mathbf{k}\uparrow}}{E_{\mathbf{k}}} \right), \end{aligned} \quad (64a)$$

and $E_{\mathbf{k}} = \sqrt{\xi_{\mathbf{k}\uparrow}^2 + |\Delta_\uparrow(\mathbf{k})|^2}$. The spectral function is then

$$A_\uparrow(\mathbf{k}, \omega) = u_{\mathbf{k}}^2 \delta(\omega - E_{\mathbf{k}}) + v_{\mathbf{k}}^2 \delta(\omega + E_{\mathbf{k}}). \quad (65)$$

As we have discussed, the p -wave ground state is expected to have $p_x + ip_y$ symmetry, given by Eq. (54)[40, 47, 54]. A full calculation of the RF lineshape requires $\Delta(k^2)$ for all k , a difficult self-consistency problem that is beyond the scope of this work. We proceed by simply assuming $\Delta(k^2) = \Delta_0$, i.e., a constant value. At zero temperature and using Eqs. (64a), (65), and (54) the momentum integrals in Eq. (61) can be done exactly, although the result is too unwieldy to present here. Figure 12 shows the resulting RF line shape at unitarity. In this plot we chose $\Delta_0 \simeq k_B T_c$, assuming the magnitude of the pairing gap reflects the transition temperature (with the latter given by $T_c \simeq .03\epsilon_{F\uparrow}/k_B$, a typical maximum value in Fig. 10). Such an estimate is more conservative than the rather large estimate found in Sec. V. As can be seen from Fig. 12, unlike the s -wave state, which has a hard gap for $\omega \lesssim \Delta_0^2/\epsilon_{F\uparrow}$, the RF line shape of this p -wave state remains non-zero for all ω , due to the nodes in the pairing gap. In principle one could use this to detect the p -wave phase of imbalanced Fermi gases. One issue, however, is the small magnitude of the peak position in the energy in Fig. 12, which occurs at a scale of order $\Delta_0^2/\epsilon_{F\uparrow}$ (rather

than at Δ_0). To see whether p -wave pairing is truly observable, we need a good estimate of the low-temperature pairing gap in this phase.

B. Density correlations

The use of spatial correlations in the density of the free expanded gas, or density-density correlations, as a tool to probe the order of the superfluid state of ultra-cold atomic systems was put forth in Ref. 49. As free expansion of the density probes the momentum distribution of the trapped system, spatial correlations of this expansion probes correlations in momentum space. It is these momentum correlations of the superfluid state that are a direct consequence of the Cooper pairing.

Theoretically the quantity of interest is the equal time density-density correlation function of the spins- \uparrow

$$D(\mathbf{r}, \mathbf{r}', t) = \text{Tr} \rho_{\text{trap}} \delta \hat{n}_{\uparrow}(\mathbf{r}, t) \delta \hat{n}_{\uparrow}(\mathbf{r}', t), \quad (66)$$

where $\delta \hat{n}_{\uparrow}(\mathbf{r}) = \hat{n}_{\uparrow}(\mathbf{r}) - \langle \hat{n}_{\uparrow}(\mathbf{r}) \rangle$ and ρ_{trap} is the equilibrium density matrix of the trapped system, i.e., superfluid, while the time evolution of the operators is given by free un-trapped Hamiltonian. As the spins- \downarrow are assumed unpaired, their momentum correlations are essentially featureless and won't be included. Neglecting the inhomogeneity caused by the trapping, we take the density matrix to be given by the zero temperature BCS state,

$$|\Psi_{\text{BCS}}\rangle = \prod_{\mathbf{k}} \left(u_{\mathbf{k}} + v_{\mathbf{k}} a_{\mathbf{k}\uparrow}^{\dagger} a_{-\mathbf{k}\uparrow}^{\dagger} \right) |\text{vac}\rangle, \quad (67)$$

with the coherence factors given by Eq. (64a) above. Within this approximation and assuming the density is measured on space and times scales much larger than $k_{\text{F}\uparrow}^{-1}$ and $\epsilon_{\text{F}\uparrow}$, we find

$$D(\mathbf{r}, \mathbf{r}', t) \approx \left(\frac{m}{2\pi t} \right)^6 \sum_{\mathbf{q}, \mathbf{q}'} \phi_{\mathbf{q}}^*(\mathbf{r}m/t) \phi_{\mathbf{q}}(\mathbf{r}'m/t) \times \phi_{\mathbf{q}'}(\mathbf{r}'m/t) \phi_{\mathbf{q}'}^*(\mathbf{r}m/t) |u_{\mathbf{q}}|^2 |v_{\mathbf{q}}|^2, \quad (68)$$

where $\phi_{\mathbf{q}}(\mathbf{k})$ is the Fourier transform of the single-particle wave function of the trapped system with quantum index \mathbf{q} . Typically these will be very sharply peaked near \mathbf{k} and \mathbf{k}' , thus

$$D(\mathbf{r}, \mathbf{r}', t) \approx \left(\frac{m}{2\pi t} \right)^6 \tilde{\delta}(\mathbf{r}m/t + \mathbf{r}'m/t) |u_{\mathbf{k}(\mathbf{r})}|^2 |v_{\mathbf{k}(\mathbf{r})}|^2, \quad (69)$$

where $\tilde{\delta}(\mathbf{r})$ is essentially a broadened delta function, the form of which depends on the specific details of the trapped system. Excluding the pre-factor, the weight of the “delta function” $|u_{\mathbf{k}(\mathbf{r})}|^2 |v_{\mathbf{k}(\mathbf{r})}|^2$ provides the information about the momentum correlations with $\mathbf{k}(\mathbf{r}) = \mathbf{r}m/t$.

Experimentally one does not measure the local density in 3-space, but instead the column integrated density.

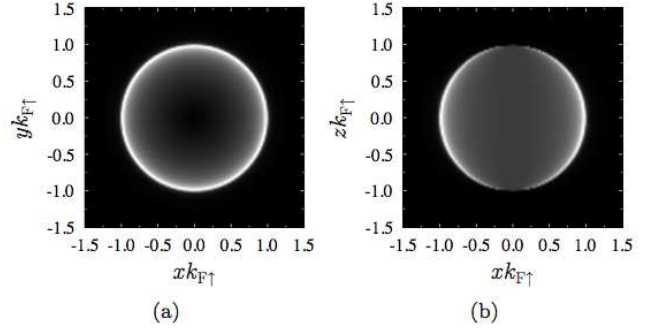


FIG. 13: The column integrated density-density correlations (70) (weight of delta function only) of a free expanded $p_x + ip_y$ superfluid with maximum gap $\Delta_0 = 0.03\epsilon_{\text{F}\uparrow}$ and symmetry axis $\hat{\mathbf{z}}$ is shown: (a) by integrating along the z -axis and (b) integrating along the y -axis. As the product of $|u_{\mathbf{k}(\mathbf{r})}|^2 |v_{\mathbf{k}(\mathbf{r})}|^2$ appearing in (70) is only appreciably nonzero near the Fermi surface, the magnitude of the correlations is maximum there. This results in the ring-shape seen in both (a) and (b).

For example if the detector is located in the x - y plane at a distance z_0 from the origin then the column integrated density-density correlation function is

$$D(\mathbf{r}_{\perp}, \mathbf{r}'_{\perp}, t) = \int_{-\infty}^{z_0} dz dz' D(\mathbf{r}, \mathbf{r}', t) \approx \left(\frac{m}{2\pi t} \right)^6 \tilde{\delta}(\mathbf{r}_{\perp}m/t + \mathbf{r}'_{\perp}m/t) \int_{-\infty}^{z_0} dz |u_{\mathbf{k}(\mathbf{r})}|^2 |v_{\mathbf{k}(\mathbf{r})}|^2, \quad (70)$$

where \mathbf{r}_{\perp} corresponds to spatial directions perpendicular to the column integration. As the p -wave breaks rotational symmetry, here chosen to be in the $\hat{\mathbf{z}}$ direction, the observed column integrated density-density correlations depends on the relative orientation of the spontaneously broken symmetry direction and the detector. Figure 13 shows the column integrated density-density correlation (weight function only) for a detector located in an x - y plane and an x - z plane for the $p_x + ip_y$ state with a gap $\Delta_0 = 0.03\epsilon_{\text{F}\uparrow}$. In Fig. 13b the p -wave nature can clearly be seen when the integrated column density is obtained by integrating along the direction that is perpendicular to the symmetry of the order parameter.

VII. CONCLUSIONS

Cold atom experiments have demonstrated the capability to study a remarkably simple many-body physics problem: That of two species of attractively interacting fermion as a function of the interatomic scattering length and relative densities of the two species. Despite the simplicity of this problem, the resulting phase diagram is quite rich, showing regions of phase separation, imbalanced superfluid, and normal Fermi liquid.

The question we pursue here is, why aren't there more phases of imbalanced Fermi gases? Indeed, experiments on imbalanced Fermi gases observe the absence of any broken symmetry phases for a large range of parameters. For example, at unitarity, Ref. [38] finds that phase separation vanishes above $P \simeq 0.36$. Are there truly no broken-symmetry ground states of imbalanced Fermi gases over the range of polarization values $0.36 \lesssim P < 1$, or do other phases lurk at low temperatures in this strongly interacting system?

This paper partially addresses such questions by proposing that, in the large imbalance region the true ground state is a p -wave superfluid of the spin- \uparrow fermions, with the order setting in below a temperature, T_c , plotted in Fig. 1. Important questions for further work include obtaining more accurate estimates for T_c and studying the p -wave gap equation at low T , and determining the transition temperature for the onset of pairing for the spins- \downarrow in the unitary regime (and finding how this onset modifies the properties of the spin- \uparrow Cooper pairs). An additional question concerns finding more experimental signatures of the onset of p -wave pairing, to help ascer-

tain the validity of this scenario.

From a general point of view, a natural question is whether other phases, such as higher-angular momentum superfluids or FFLO phases intervene in the $T \rightarrow 0$ limit of imbalanced Fermi gases. Since the p -wave interaction becomes repulsive for small imbalance (below the dashed line in Fig. 8), it is likely that other angular momentum channels can become dominant in this regime. Additionally, although the window of FFLO stability is extremely thin for the simplest FFLO-type state within mean-field theory, it is possible that generalized FFLO states, within theoretical approaches that go beyond mean-field theory, can lead to a wider regime of FFLO stability [21–23].

Acknowledgments

KRP would like to thank Hartmut Hafermann and Herbert Fotso for useful discussions. This work was supported by the Louisiana Board of Regents, under grant LEQSF (2008-11)-RD-A-10.

-
- [1] W. Ketterle and M. Zwierlein, “Making, probing and understanding ultracold Fermi gases”, in *Ultracold Fermi Gases*, Proceedings of the International School of Physics “Enrico Fermi”, Course CLXIV, Varenna, 20 - 30 June 2006, edited by M. Inguscio, W. Ketterle, and C. Salomon.
 - [2] V. Gurarie and L. Radzihovsky, *Ann. of Phys.* **322**, 2 (2007).
 - [3] I. Bloch, J. Dalibard, W. Zwerger, *Rev. Mod. Phys.* **80**, 885 (2008).
 - [4] S. Giorgini, L.P. Pitaevskii, and S. Stringari, *Rev. Mod. Phys.* **80**, 1215 (2008).
 - [5] M.W. Zwierlein, A. Schirotzek, C.H. Schunck, and W. Ketterle, *Science* **311**, 492 (2006).
 - [6] G.B. Partridge, W. Li, R.I. Kamar, Y.-A. Liao, R.G. Hulet, *Science* **311**, 503 (2006).
 - [7] Y. Shin, M. W. Zwierlein, C. H. Schunck, A. Schirotzek, W. Ketterle, *Phys. Rev. Lett.* **97**, 030401 (2006).
 - [8] G.B. Partridge, W. Li, Y. A. Liao, R. G. Hulet, M. Haque, and H.T.C. Stoof, *Phys. Rev. Lett.* **97**, 190407 (2006).
 - [9] P.F. Bedaque, H. Caldas, and G. Rupak, *Phys. Rev. Lett.* **91**, 247002 (2003).
 - [10] D.T. Son and M.A. Stephanov, *Phys. Rev. A* **74**, 013614 (2006).
 - [11] C.-H. Pao, S.-T. Wu, and S.-K. Yip, *Phys. Rev. B* **73**, 132506 (2006).
 - [12] D.E. Sheehy and L. Radzihovsky, *Phys. Rev. Lett.* **96**, 060401 (2006).
 - [13] C. Chien, Q. Chen, Y. He, and K. Levin, *Phys. Rev. Lett.* **97**, 090402 (2006).
 - [14] M.M. Parish, F.M. Marchetti, A. Lamacraft, and B.D. Simons, *Nat. Phys.* **3**, 124 (2007).
 - [15] D.E. Sheehy and L. Radzihovsky, *Ann. of Phys.* **322**, 1790 (2007).
 - [16] D.E. Sheehy and L. Radzihovsky, *Phys. Rev. B* **75**, 136501 (2007).
 - [17] L. Radzihovsky and D.E. Sheehy, *Rep. Prog. Phys.* **73**, 076501 (2010).
 - [18] F. Chevy and C. Mora, *Rep. Prog. Phys.* **73**, 112401 (2010).
 - [19] P. Fulde and R. A. Ferrell, *Phys. Rev.* **135**, A550 (1964).
 - [20] A.I. Larkin and Yu.N. Ovchinnikov, *Zh. Eksp. Teor. Fiz* **47**, 1136 (1964) [*Sov. Phys. JETP* **20**, 762 (1965)].
 - [21] N. Yoshida, and S.-K. Yip, *Phys. Rev. A* **75**, 063601 (2007).
 - [22] L. Radzihovsky and A. Vishwanath, *Phys. Rev. Lett.* **103**, 010404 (2009).
 - [23] L. Radzihovsky, *Phys. Rev. A* **84**, 023611 (2011).
 - [24] Y. Liao, A.S.C. Rittner, T. Paprotta, W. Li, G.B. Partridge, R.G. Hulet, S.K. Baur, and E.J. Mueller, *Nature* **467**, 567 (2010).
 - [25] C. Lobo, A. Recati, S. Giorgini, and S. Stringari, *Phys. Rev. Lett.* **97**, 200403 (2006).
 - [26] M. Punk and W. Zwerger, *Phys. Rev. Lett.* **99**, 170404 (2007).
 - [27] M. Veillette, E.G. Moon, A. Lamacraft, L. Radzihovsky, S. Sachdev, and D.E. Sheehy, *Phys. Rev. A* **78**, 033614 (2008).
 - [28] A. Schirotzek, C.-H. Wu, A. Sommer, and M.W. Zwierlein, *Phys. Rev. Lett.* **102**, 230402 (2009).
 - [29] S. Nascimbène et al, *Phys. Rev. Lett.* **103**, 170402 (2009).
 - [30] F. Chevy, *Phys. Rev. A* **74**, 063628 (2006).
 - [31] R. Combescot, A. Recati, C. Lobo, and F. Chevy, *Phys. Rev. Lett.* **98**, 180402 (2007).
 - [32] R. Combescot and S. Giraud, *Phys. Rev. Lett.* **101**, 050404 (2008).
 - [33] W. Kohn and J. M. Luttinger, *Phys. Rev. Lett.* **15**, 524 (1965).
 - [34] J. M. Luttinger, *Phys. Rev.* **150**, 202 (1966).

- [35] A. Bulgac, M. Forbes, A. Schwenk, Phys. Rev. Lett **97**, 020402 (2006).
- [36] K.R. Patton and D.E. Sheehy, Phys. Rev. A **83**, 051607(R) (2011).
- [37] A. Bulgac and S. Yoon, Phys. Rev. A **79**, 053625 (2009).
- [38] Y. Shin, C.H. Schunck, A. Schirotzek, and W. Ketterle, Nature **451**, 689 (2008).
- [39] R. Liao and K.F. Quader, Phys. Rev. B **76**, 212502 (2007).
- [40] Y. Nishida, Ann. Phys. **324**, 897 (2009).
- [41] S. Giraud and R. Combescot, Phys. Rev. A **85**, 013605 (2012).
- [42] K.B. Gubbels, M.W.J. Romans and H.T.C. Stoof Phys. Rev. Lett. **97**, 210402 (2006).
- [43] D.E. Sheehy, Phys. Rev. A **79**, 033606 (2009).
- [44] G.D. Mahan, *Many Particle Physics*, Plenum, New York, 1990.
- [45] J.M. Luttinger and J.C. Ward, Phys. Rev. **118**, 1417 (1960).
- [46] S. Sachdev and K. Yang, Phys. Rev. B **73**, 174504 (2006).
- [47] P.W. Anderson and P. Morel, Phys. Rev. **123**, 1911 (1961).
- [48] C. Chin, M. Bartenstein A. Altmeyer, S. Riedl, S. Jochim, J.H. Denschlag, and R. Grimm, Science **305**, 1128 (2004).
- [49] E. Altman, E. Demler, and M.D. Lukin, Phys. Rev. A **70**, 013603 (2004).
- [50] M. Greiner, C.A. Regal, J.T. Stewart, and D.S. Jin, Phys. Rev. Lett. **94**, 110401 (2005).
- [51] M.W. Zwierlein, J.R. Abo-Shaeer, A. Schirotzek, C.H. Schunck, and W. Ketterle, Nature **435**, 1047 (2005).
- [52] C. Zhang, S. Tewari, R.M. Lutchyn, and S. Das Sarma, Phys. Rev. Lett. **101**, 160401 (2008).
- [53] Q. Chen, Y. He, C. Chien, and K. Levin, Rep. Prog. Phys. **72**, 122501 (2009).
- [54] V. Gurarie, L. Radzihovsky, and A.V. Andreev, Phys. Rev. Lett. **94**, 230403 (2005).
- [55] Y. Shin, A. Schirotzek, C.H. Schunck, and W. Ketterle, Phys. Rev. Lett. **101**, 070404 (2008).